Time-locking of single-unit activity to electrical stimulation: a possible signature of human epileptogenic cortex

Andrei Barborica[1,2], Cristian Donos[1,3], Ioana Mindruta[4], Jean Ciurea[5]

[1]Physics Department, University of Bucharest, Bucharest, Romania, [2]FHC Inc, Bowdoin, ME, United States of America, [3]Epilepsy Center, University Hospital of Freiburg, Freiburg, Germany
[4]Neurology Department, University Emergency Hospital, Bucharest, Romania, [5]Neurosurgery Department, Bagdasar-Arseni Emergency Hospital, Bucharest, Romania, E-mail: andrei.barborica@fizica.unibuc.ro

Background

As the single-unit activity is ultimately the underlying source of the EEG signals, advances in understanding the electrical activity at the single-neuron level allow us to elucidate EEG signal features originating from the epileptic cortex. Hypersynchrony of spontaneous neuronal firing within large population of neurons has been considered to be a distinctive characteristic of the ictal discharges. However, synchronization of unit activity in humans with electrical stimuli has been investigated in less detail.

Objectives

We are aiming at probing the susceptibility to synchronization of epileptogenic tissue by recording single-unit response to intraoperative electrical stimulation applied to the seizure onset zone (SOZ) in patients undergoing resective surgery for drug-resistant epilepsy.

Patients and Methods

We performed SEEG presurgical evaluation of 12 patients with drug-resistant focal epilepsy to locate the seizure-onset zone (SOZ) and delineate the area to be resected.

Patient	Sex	Age	Pathology	Epilepsy	SOZ
1	F	32	Type I FCD	Temporal	Mesial structures
2	M	46	Sclerosis	Mesio-temporal	Amygdala
3	M	39	MCD	Temporo-occipital	Basal
4	M	47	DNET	Temporal	Middle temporal gyrus
5	F	40	Type II B FCD	Prefrontal	Dorsolateral prefrontal cortex
6	F	35	Gliosis	Mesio-temporal	Amygdala
7	F	25	Type II FCD	Temporal	Temporal pole
8	F	46	Type II FCD	Temporal	Temporal pole
9	M	33	Type I FCD	Frontal	Anterior cingulate cortex
10	M	28	Type I FCD	Temporal	Hippocampus
11	F	25	Type I FCD	Temporal	Entorhinal cortex
12	M	53	Cavernoma	Frontal	Frontal pole

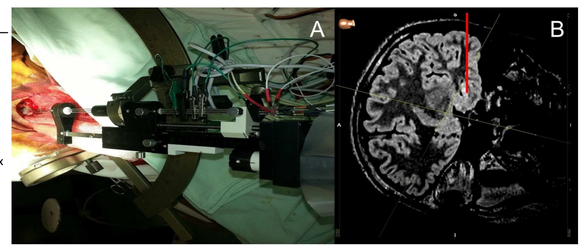

Figure 1. A) Acute microelectrode recording setup using clinical microelectrodes, stereotactic positioning, stimulation and recording instrumentation commonly used for functional mapping in deep brain stimulation procedures; B) Electrode trajectory in patient 10, shown in red, passing through several sulci in temporo-basal epileptogenic cortex and targeting the hippocampus, which is the seizure onset zone.

Prior to the resective surgery, we are stereotactically inserting three microelectrodes, spaced 2mm apart, in a linear configuration, following a trajectory targeting SOZ. Standard clinical microelectrodes and equipment used in functional mapping for deep brain stimulation implantations was used. Bipolar electrical stimulation is applied in most cases between the two outer macro contacts of the electrodes, while recording the unit activity on the center microelectrode, located 3 mm deeper than the macro contacts. Constant current 0.5 to 1 mA biphasic pulses, 0.3 ms pulse width, frequency 1, 10, 30, 60 were applied for 30 s using a clinical recording and stimulating system (Guideline LP+, FHC Inc, Bowdoin, ME). The interval before, between and after each electrical stimulation epoch was at least 30 seconds.

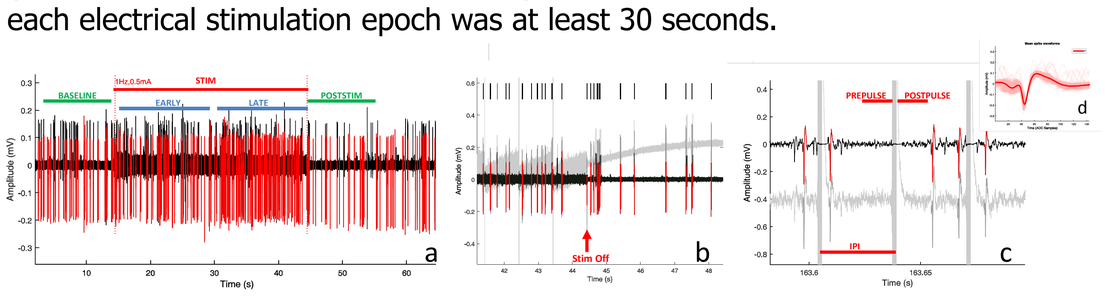

Figure 2. Illustration of the recording while stimulating, stimulus artifact removal and spike discrimination. a) the 1-Hz stimulation epoch recorded in patient 7 with discriminated neurons highlighted in red; b) a detail of the end of the stimulation epoch, showing the raw signal (gray) and the filtered signal. One has to note the noise band during stimulation that is significantly reduced. c) example of neurons recovered from the 30-Hz stimulation epoch. The blanking interval is 4.16 ms, accounting for 4.16% of the inter-pulse interval at 10 Hz and 25% at 60 Hz. d) mean spike waveform of the neuron presented in a), b) and c).

In order to remove the stimulation artifact, we used SALPA algorithm (Wagenaar and Potter, 2002). In addition, the noise introduced by the stimulator, correlated across channels, has been removed by using an adaptive noise cancellation filter (Widrow, 1975) using as reference the signal on one of the other microelectrode. Simultaneously sampled channels and built-in stimulation unit sharing the same clock as the recording unit resulted in a stimulation artifact without any pulse to pulse variability, therefore facilitating artifact removal (Hashimoto et al., 2002). Spike sorting was performed using FIND toolbox (Meier et al., 2008).

Firing rate modulation indexes were calculated for a) assessing the effect of electrical stimulation, defined as the difference between mean firing rate during stimulation and the pre-stimulation baseline, divided by the sum of the two; b) assessing the time course of the stimulation, defined like the previous index, but using the early and late responses during each stimulation epoch

$$MI_{STIM} = \frac{R_{STIM} - R_{BASELINE}}{R_{STIM} + R_{BASELINE}} \qquad MI_{BUILDUP} = \frac{R_{LATE} - R_{EARLY}}{R_{LATE} + R_{EARLY}} \qquad TLI = \frac{R_{POSTPULSE} - R_{PREPULSE}}{R_{POSTPULSE} + R_{PREPULSE}}$$

At the level of each stimulation pulse, we have calculated the time-locking index, defined as the difference between the activity in half of the inter-ulse interval (IPI) following each pulse and the activity in the half IPI preceding each stimulation pulse, divided by the sum of two.

A representation of the firing in complex plane has been performed by introducing a complex representation of the spikes:

$$z_i = \cos(2\pi f_s t_i) + j\sin(2\pi f_s t_i) \qquad |z_i| = 1 \qquad \theta_i = \arg(z_i) = \arctan\left(\frac{\sin(2\pi f_s t_i)}{\cos(2\pi f_s t_i)}\right)$$

Vector strength index (Goldberg and Brown, 1969) has been calculated for 2-s bins and for the entire stimulation interval:

$$z_{VSI} = \frac{1}{n}\sum_{i=1}^{n} z_i$$

$$VSI = |z_{VSI}| = \left|\frac{1}{n}\sum_{i=1}^{n} z_i\right| = \frac{1}{n}\sqrt{\left(\sum_{i=1}^{n}\cos(2\pi f_s t_i)\right)^2 + \left(\sum_{i=1}^{n}\sin^2(2\pi f_s t_i)\right)^2} \qquad \theta_{VSI} = \arg(z_{VSI}) = \arctan\left(\frac{\sum_{i=1}^{n}\sin(2\pi f_s t_i)}{\sum_{i=1}^{n}\cos(2\pi f_s t_i)}\right)$$

Results

We have recorded a total of 21 neurons in 12 patients. This represents a subset of neurons having most prominent action potentials among multiple units that have been identified by the spike-sorting software. A number of 15 neurons were located in epileptogenic tissue (in SOZ and adjacent areas), whereas 6 were located in normal tissue. A total of 81 stimulation trains of different frequencies and amplitudes were applied (58 in EZ, 23 in non-pathological tissue).

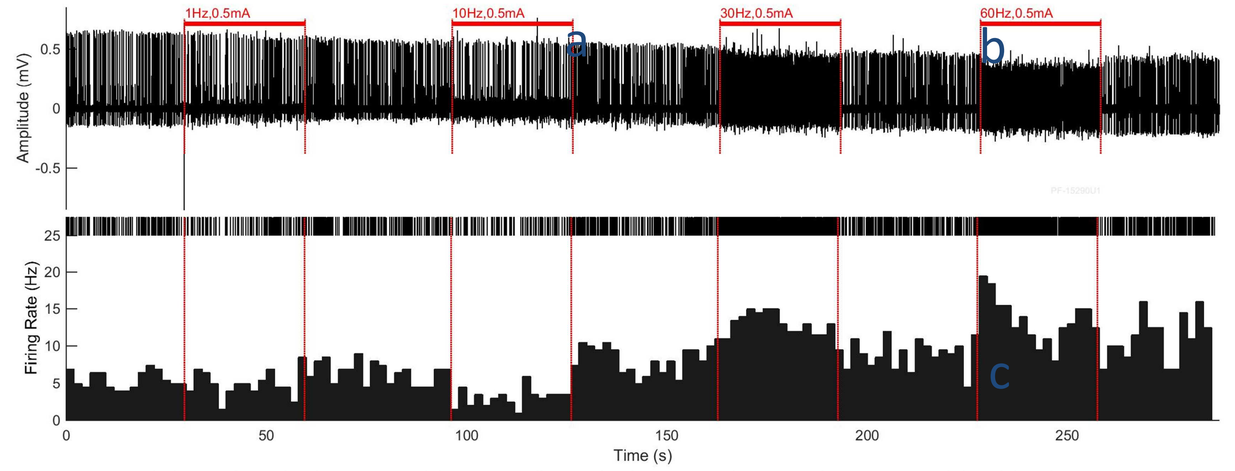

Figure 3. Recorded waveform (top), raster and histogram (bottom) of a neuron having a firing rate modulated by the application of 0.5 mA stimulation pulses, located in epileptogenic cortex of patient 10 (temporo-basal cortical dysplasia). The baseline mean firing rate (6.30 Hz) is little modified by the 1 Hz and 10 Hz stimulation (4.95 Hz and 3.23 Hz, respectively), whereas at higher frequencies, it increases to 14.97 and 18.35 Hz for 30 and 60 Hz stimulation, respectively.

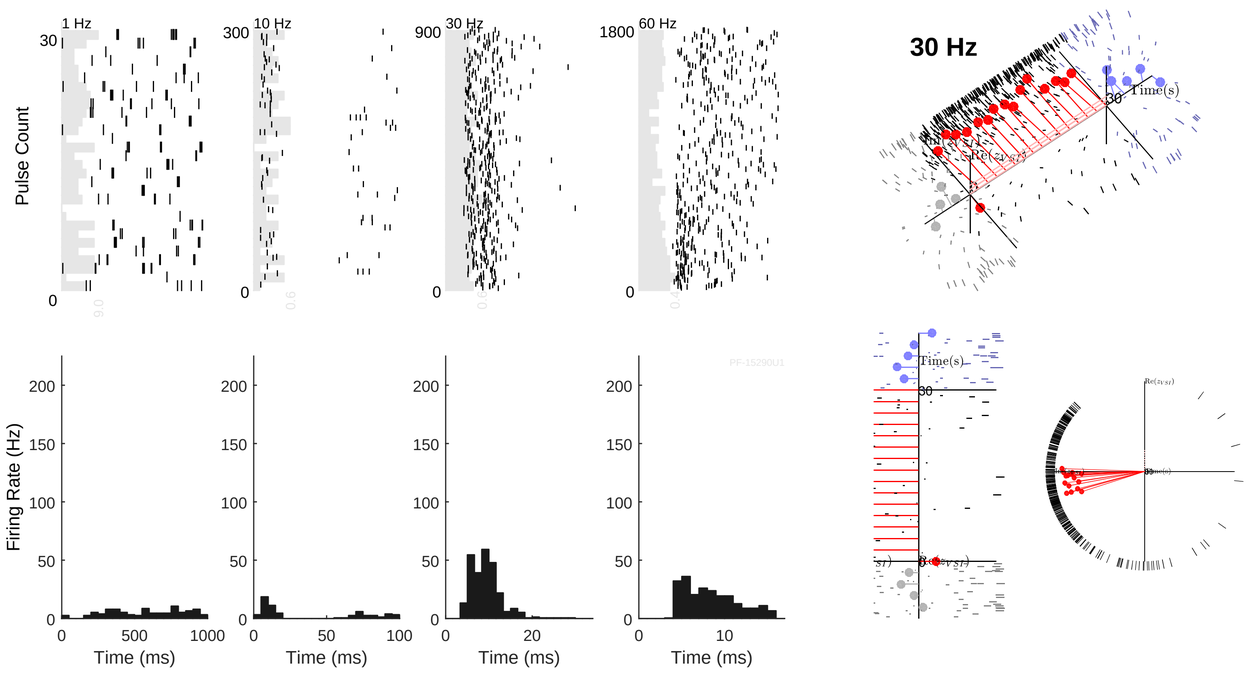

Figure 4. Peri-stimuls histograms (bottom row) and rasters (top row) of the same neuron as in figure 3. The time-locking index takes values of -17.2%, 25.9%, 93.5%, and 33.3% for the 1, 10, 30 and 60 Hz stimulation frequencies, respectively. The light gray histograms behind the rasters illustrate the variation of the spike count per stimulation cycle. In the right panels, the 3D representation of the complex spikes and vector strength indices for 30 Hz stimulation, calculated over 2 sec bins

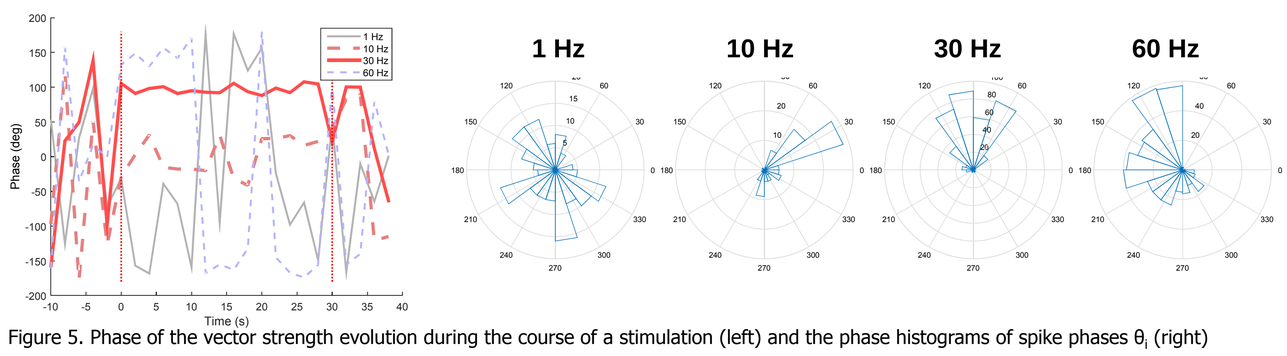

Figure 5. Phase of the vector strength evolution during the course of a stimulation (left) and the phase histograms of spike phases θ_i (right)

At the population level, a 3-way Anova analysis of the firing rate (MI_{STIM}, $MI_{BUILDUP}$) showed a significant dependence on the patient ($p<0.05$) but non-significant dependence on frequency and epileptogenicity ($p>0.1$). By contrast, time-locking (TLI) depended significantly on all factors: patient ($p<0.001$), epileptogenicity ($p<0.05$), and frequency ($p<0.01$).

	Epileptogenicity	All frequencies	1 Hz	10 Hz	30 Hz	60 Hz
MI_{STIM}	All neurons	0.10±0.49, n=81	0.13±0.50, n=21	-0.02±0.38, n=21	0.20±0.54, n=21	0.07±0.55, n=18
	EZ	0.10±0.51, n=58	0.12±0.50, n=15	-0.08±0.35, n=15	0.20±0.57, n=15	0.15±0.61, n=13
	non-EZ	0.09±0.46, n=23	0.16±0.54, n=6	0.11±0.46, n=6	0.19±0.50, n=6	-0.14±0.33, n=5
$MI_{BUILDUP}$	All neurons	-0.09±0.37, n=81	0.03±0.37, n=21	-0.08±0.29, n=21	-0.16±0.25, n=21	-0.17±0.54, n=18
	EZ	-0.13±0.40, n=58	-0.01±0.33, n=15	-0.13±0.30, n=15	-0.16±0.27, n=15	-0.25±0.62, n=13
	non-EZ	0.02±0.30, n=23	0.15±0.47, n=6	0.05±0.21, n=6	-0.15±0.22, n=6	0.01±0.18, n=5
TLI	All neurons	0.15±0.42, n=81	-0.10±0.25, n=21	0.25±0.51, n=21	0.26±0.45, n=21	0.20±0.29, n=18
	EZ	0.21±0.48, n=58	-0.13±0.28, n=15	0.33±0.59, n=15	0.36±0.50, n=15	0.28±0.29, n=13
	non-EZ	0.01±0.11, n=23	-0.02±0.11, n=6	0.05±0.05, n=6	0.03±0.13, n=6	-0.03±0.15, n=5

Table 2. Firing rate modulation index due to the application of electrical stimulation, activity buildup index during stimulation epoch and time-locking to stimulation pulses index. The number n of trials or neurons in each category are listed along with mean±SD index values.

A 3-way Anova on the index values in EZ only, with patient, pathology and frequency as factors, showed no significant role of the specific pathology in any modulation index or timelocking index ($p>0.3$).

Conclusions

- Our study shows that susceptibility to hypersynchronization of neurons in epileptogenic cortex can be probed with electrical stimulation.
- There is a strong frequency-dependence of the effects, as stimulation pulses with low repetition rate generally fail to entrain neural activity.
- Time-locking, but not firing rate, correlates with tissue epileptogenicity. Susceptibility for time locking to stimulation pulses may therefore be considered as a single-unit signature of the pathological cortex.

Acknowledgments

We would like to thank Alin Rasina, MD, Bogdan Balanescu, MD, Ana Ciurea, MD for their contribution to the surgical procedures and to Mihai Maliia, MD, Irina Popa, MD, Sabina Ene, BSc, for their contribution to the presurgical evaluation of the patients and data collection. This work was supported by Romanian government UEFISCDI research grant PN-II-IDPCE-2011-3-0240.

References

Goldberg JM, Brown PB. Response of binaural neurons of dog superior olivary complex to dichotic tonal stimuli: some physiological mechanisms of sound localization. J Neurophysiol 1969; 32: 613-36.

Hashimoto T, Elder CM, Vitek JL. A template subtraction method for stimulus artifact removal in high-frequency deep brain stimulation. J Neurosci Methods 2002; 113: 181-6.

Meier R, Egert U, Aertsen A, Nawrot MP. FIND - a unified framework for neural data analysis. Neural Netw 2008; 21:1085-93.

Wagenaar DA, Potter SM. Real-time multi-channel stimulus artifact suppression by local curve fitting. J Neurosci Methods 2002; 120: 113-20.

Widrow B, Glover JR, McCool JM, Kaunitz J, Williams CS, Hearn RH, et al. Adaptive Noise Cancelling: Principles and Applications. Proc IEEE 1975; 63: 1692-716.